AD-A048 873 ARTEC ASSOCIATES INC HAYWARD CALIF F/G 19/4
DEVELOPMENT OF HIGH ENERGY DENSITY SIMULATOR.(U)
JUN 77 D W BAUM, W L SHIMMIN, S P GILL DNA001-75-C-0271
UNCLASSIFIED FR-120 DNA-4371F NL

1 OF 1
ADA048873

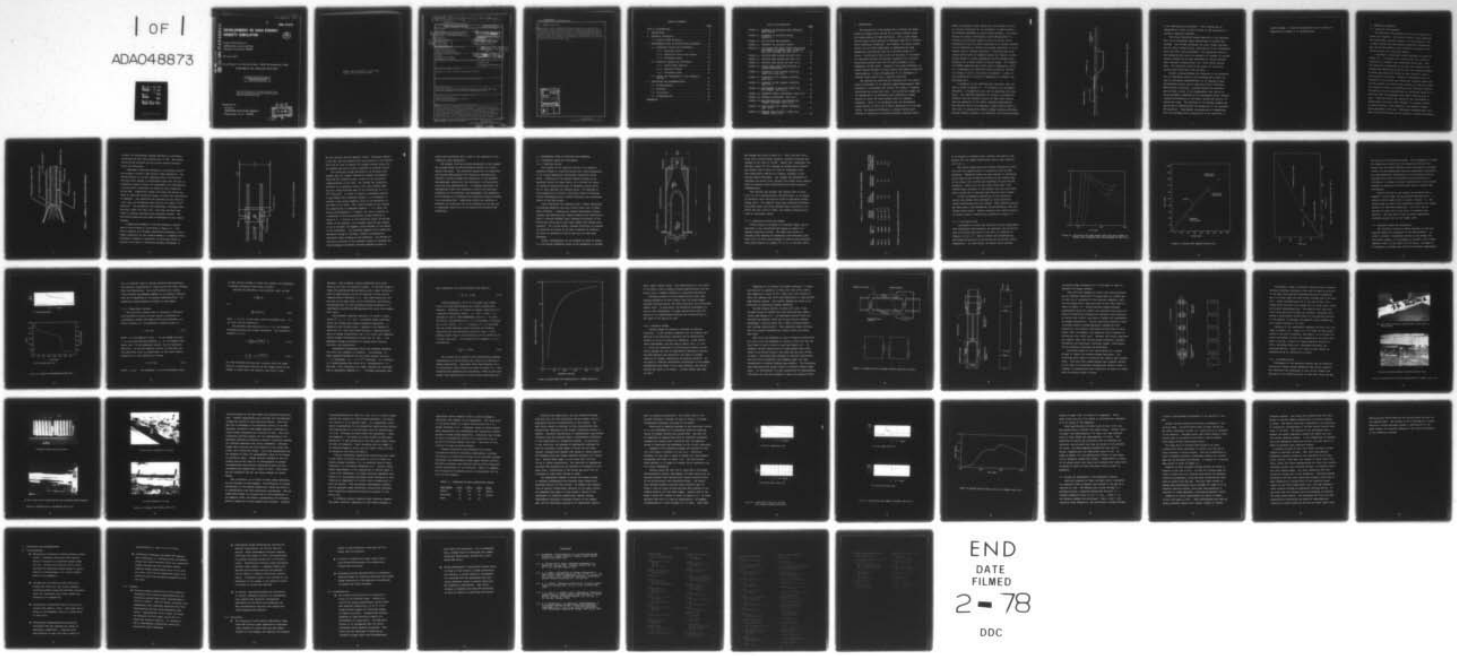

END
DATE FILMED
2-78
DDC

AD-E300 072

DNA 4371F

DEVELOPMENT OF HIGH ENERGY DENSITY SIMULATOR

(12)

Artec Associates Inc.
26046 Eden Landing Road
Hayward, California 94545

15 June 1977

Final Report for Period 15 April 1975—15 December 1976

CONTRACT No. DNA 001-75-C-0271

APPROVED FOR PUBLIC RELEASE;
DISTRIBUTION UNLIMITED.

THIS WORK SPONSORED BY THE DEFENSE NUCLEAR AGENCY UNDER RDT&E RMSS CODES B344075464 Y99QAXSD07018 AND B344076464 Y99QAXSD07018 H2590D.

Prepared for
Director
DEFENSE NUCLEAR AGENCY
Washington, D. C. 20305

Destroy this report when it is no longer needed. Do not return to sender.

(18) DNA, SBIE (19) 4371F, AD-E300 072

UNCLASSIFIED

SECURITY CLASSIFICATION OF THIS PAGE *(When Data Entered)*

REPORT DOCUMENTATION PAGE

READ INSTRUCTIONS BEFORE COMPLETING FORM

1. REPORT NUMBER: DNA 4371F
2. GOVT ACCESSION NO.:
3. RECIPIENT'S CATALOG NUMBER:

4. TITLE (and Subtitle): (6) DEVELOPMENT OF HIGH ENERGY DENSITY SIMULATOR.

5. TYPE OF REPORT & PERIOD COVERED: (3) Final Report. [redacted] 15 Apr 75—15 Dec 76

6. PERFORMING ORG. REPORT NUMBER: (14) FR-120

7. AUTHOR(s): (10) Dennis W. Baum, W. Lee Shimmin, Stephen P. Gill

8. CONTRACT OR GRANT NUMBER(s): (15) DNA 001-75-C-0271 new

9. PERFORMING ORGANIZATION NAME AND ADDRESS:
Artec Associates Inc.
26046 Eden Landing Road
Hayward, California 94545

10. PROGRAM ELEMENT, PROJECT, TASK AREA & WORK UNIT NUMBERS: (16) Subtask Y99QAXSD070-18 (17) D070

11. CONTROLLING OFFICE NAME AND ADDRESS: (11)
Director
Defense Nuclear Agency
Washington, D.C. 20305

12. REPORT DATE: 15 Jun [redacted]77 (12) 59p.

13. NUMBER OF PAGES: 62

14. MONITORING AGENCY NAME & ADDRESS *(if different from Controlling Office)*:

15. SECURITY CLASS *(of this report)*: UNCLASSIFIED

15a. DECLASSIFICATION/DOWNGRADING SCHEDULE:

16. DISTRIBUTION STATEMENT *(of this Report)*

Approved for public release; distribution unlimited.

17. DISTRIBUTION STATEMENT *(of the abstract entered in Block 20, if different from Report)*

18. SUPPLEMENTARY NOTES

This work sponsored by the Defense Nuclear Agency under RDT&E RMSS Codes B344075464 Y99QAXSD07018 and B344076464 Y99QAXSD07018 H2590D.

19. KEY WORDS *(Continue on reverse side if necessary and identify by block number)*

Pulse Power Generation
Explosive Magnetohydrodynamic Generator
Nuclear Weapon Simulation

20. ABSTRACT *(Continue on reverse side if necessary and identify by block number)*

This study was an experimental investigation of the feasibility of an explosive MHD pulsed electric power generator. The electrical energy, when reconverted into thermal energy with a large exploding wire, will yield very high energy densities (temperature 10 eV - 100 eV) suitable for nuclear weapon simulation in large scale explosive field tests. The key technical problem was seen as fast (< 100 microsecond) self-excitation of a low inductance field coil to full power field strength of about 50 tesla.

DD FORM 1 JAN 73 1473 EDITION OF 1 NOV 65 IS OBSOLETE

UNCLASSIFIED

SECURITY CLASSIFICATION OF THIS PAGE *(When Data Entered)*

408 296

20. ABSTRACT (Continued)

Experimental results demonstrate MHD power production and partial self-excitation. Lower than expected electrical conductivity prevented complete self-excitation and full power operation. Achieved field amplification was 20 dB (to 3.7 tesla) instead of 43 dB (50 tesla) required for full power. Achieved power was in excess of 200 megawatts. Recommendations for further work to resolve the conductivity problem or minimize its effect on the field amplification process are made.

TABLE OF CONTENTS

LIST OF ILLUSTRATIONS

1. INTRODUCTION

The objective of this program was to develop and demonstrate an energy source having up to several hundred times the energy density of high explosives. Such a high energy density source would provide an important addition to nuclear burst simulation technology. For example, the source energy density is of primary importance in simulating the high temperature ablating gas flow for a nuclear source in a trench. Situations in which the size and mass of the source are important include the airblast coupling from a shallow penetrating nuclear burst and the bubble dynamics of an underwater nuclear burst. Because of the large difference in energy density between a nuclear device and chemical explosive (approximately 4 orders of magnitude) it is inadequate to simulate these events with a chemical explosive.

The program was specifically concerned with the experimental development of an explosive magnetohydrodynamic (MHD) generator to concentrate and convert the energy of chemical explosives into electrical form. The electrical energy can be transmitted to an exploding wire achieving an energy density at least 100 times greater than the chemical explosive. While it is recognized that the anticipated energy density is still not a direct simulation of a nuclear source, the expected difference in energy density would provide an opportunity to perform airblast coupling experi-

ments at shallower burial depths than now possible as well as provide information on the dependence of ground motion and airblast phenomena on source energy density. The unique feature of using an explosively driven MHD generator to provide the electrical energy is that the device can be fabricated in any size scale requiring up to several hundred tons of explosive to simulate the energy equivalent of up to several tons of chemical explosive. Alternate high power energy sources such as capacitor banks are limited in total stored energy to several megajoules and are prohibitively expensive for a large amount of stored energy. For example the AURORA capacitor bank stores about 5 megajoules, which at a 2 megajoule per pound TNT yield equivalence contains the energy of only 2 1/2 pounds of explosive. A goal of this program was to deliver 20 megajoules of energy to an exploding wire.

A schematic of the exploding wire simulator test concept is shown in Figure 1.1. It consists of an explosive generator, a transmission line, and an exploding wire simulator. The explosive generator is located a considerable distance from the simulator source so that blast effects from the generator do not affect simulator measurements. The required size of the generator, which directly affects test cost, is governed by overall energy coupling efficiency between chemical energy in the explosive and delivered energy

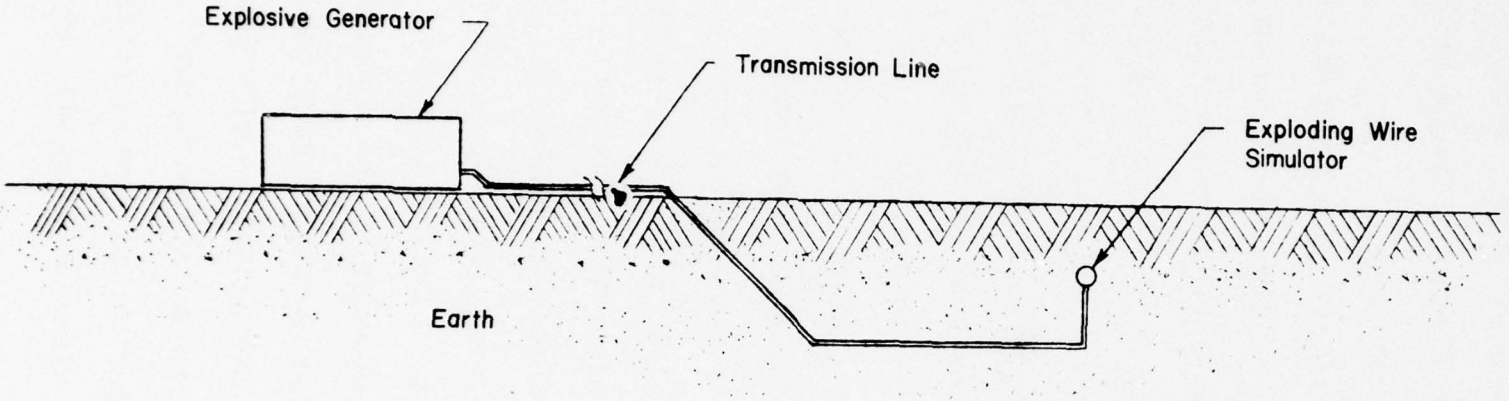

FIGURE 1.1 SCHEMATIC OF EXPLODING WIRE SIMULATOR TEST CONCEPT

in the exploding wire simulator. This coupling may be expressed as a ratio of yield (pounds of TNT equivalent) to pounds of explosive required.

The actual electrical energy deposited in the exploding wire can be determined using measurements of current and voltage. This energy represents the total energy available for air blast, ground motion, vaporization of the surrounding media and other source phenomena. The equivalent yield of the exploding wire source is typically of interest in nuclear effects studies and is best determined by fitting obtained data (airblast, ground motion, etc.) with scaled nuclear data. The equivalent yield of the source is the scaled nuclear yield which best fits the data.

Overall coupling between the explosive in the generator and the equivalent yield of the exploding wire source can only be determined experimentally, as it depends on many interrelated factors such as explosive driver efficiency, MHD generator efficiency, coupling between the generator and the load, losses in the transmission line, and so on. Rough estimates, supported by the discussions below, indicate coupling efficiencies in the range 5 pounds per pound to 50 pounds per pound. The objective of the present program was restricted to demonstrating the feasibility of the explosive MHD generator. Experimental investigation of transmission line and exploding wire coupling will be the objective of

later programs. A specific program goal was to deliver 20 megajoules of energy to an exploding wire.

2. TECHNICAL DISCUSSION

2.1 Explosive MHD Generator

The explosive MHD generator used in this program comprises two elements: an explosive driver, which transfers and concentrates chemical energy of a high explosive into a highly ionized and electrically conductive intermediary gas; and an MHD channel, which converts the energy of the conductive gas into electrical energy.

A schematic of explosive driver operation is shown in Figure 2.1. It consists of a tube filled with explosive enclosed in a pressure tube containing driver gas. When the explosive is detonated at one end, the expansion tube expands and impacts the pressure tube; this impact produces a moving gas seal which drives the gas forward to form a high pressure shock wave. Energy is transferred from the explosive to the driver gas because the explosive gases must do work against the driver shock pressure in order to expand. The explosive driver is potentially very efficient; maximum efficiency would be obtained when the detonation gases do so much work that the expansion tube impact velocity goes to zero. Practical limits are imposed by the requirement of maintaining a gas seal, which depends in a complex fashion on impact velocity, tube materials, and dynamic boundary layer phenomena in the gas. Reasonable extrapolations indicate that 50% efficiency can be expected; achieved efficiency

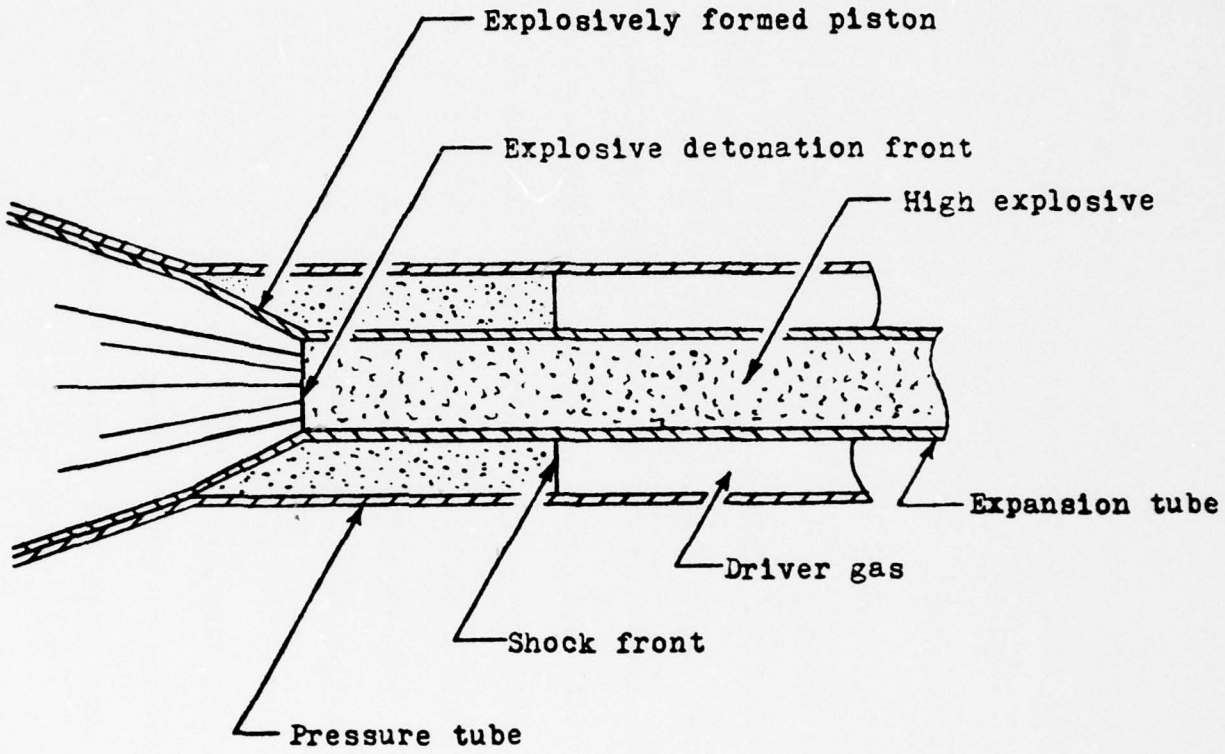

FIGURE 2.1 SCHEMATIC OF EXPLOSIVE DRIVER OPERATION

to date (no experimental program dedicated to optimizing efficiency has ever been carried out) is 25%. The conservative driver selected for the current program delivers about 10% efficiency.

Gasdynamic conditions achieved by an explosive driver are uniquely suited to MHD electric power generation. The energy density of the gas (typically about 72 kilojoules per gram total energy) is sufficiently high that the gas is completely ionized without the requirement for seed material or other exotic techniques in common use with combustion driven MHD. Conductivity ranges from about 300 mho/cm for argon to about 800 mho/cm for xenon, or about the conductivity of graphite. Gas velocities are typically on the order of 1 cm/ μsec, and mechanical power flow on the order of 10^{10} watts/cm^2. The mechanical flow conditions, including shock velocity, power flow rate, etc., have been verified many times in numerous programs using explosive drivers. The electrical properties are being investigated in the present program.

A simplified schematic of the MHD generator concept used in this program is illustrated in Figure 2.2. The device operates as a Faraday crossed-field generator, with a highly conductive hot gas flowing normal to a magnetic field. According to Maxwell's equations, an electrical field is induced in the gas in a direction mutually orthogonal to

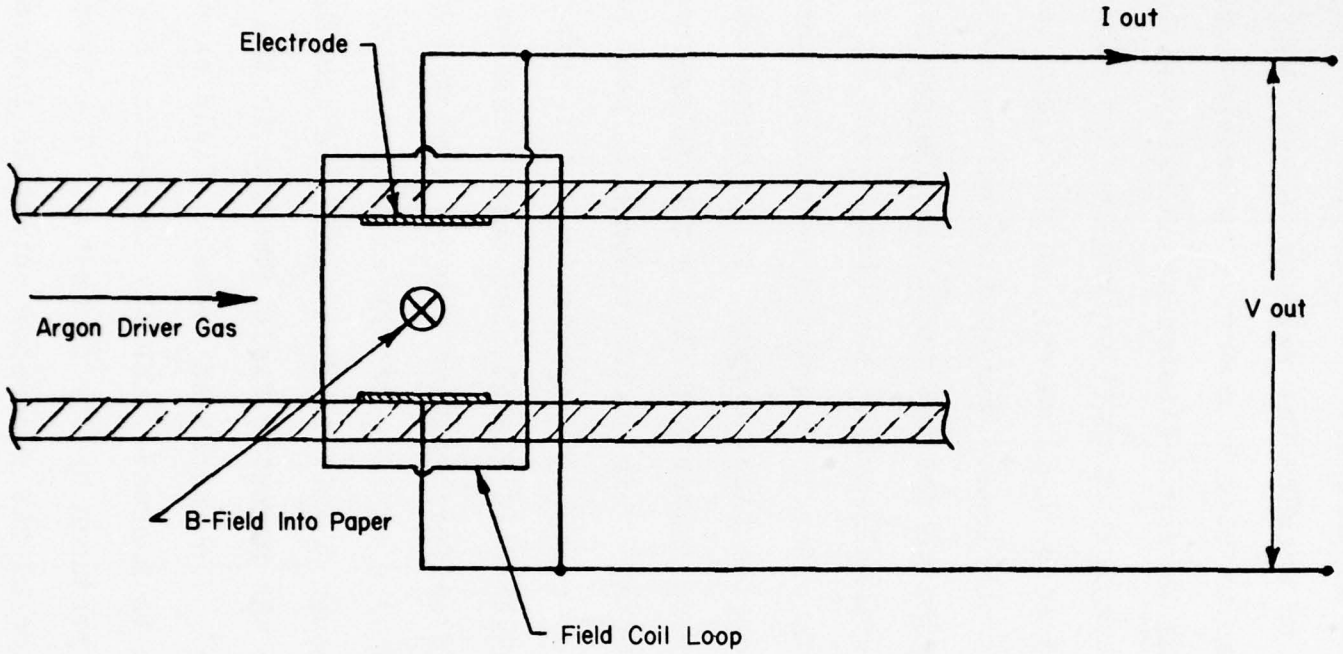

FIGURE 2.2 SELF-EXCITED MHD GENERATOR

the gas velocity and the magnetic field. Electrodes exposed to the gas flow and aligned with the direction of the electric field can be used to measure the voltage induced across the gas channel and can be used to energize an external circuit.

The electrical energy delivered to an external load depends upon the complex interaction between the magnetic field and the conductive gas, as well as the electrical characteristics of the load. For typical gas conditions produced in an explosive driver, the total thermal power per unit cross-sectional area of the flowing gas is 1.1×10^{10} watts/cm^2. In order to convert a reasonable portion of gas energy into electrical energy, it is necessary to provide a very strong magnetic field in the generator, on the order of 10 Tesla. This field strength is well beyond the capabilities of permanent magnets ($\sim$ 0.1 Tesla) and simple electromagnets ($\sim$ 1 Tesla), but can be achieved in a generator by the self-excitation process depicted in Figure 2.2. A portion of the electrical output of the generator is fed through a coil located along the gas channel so as to increase the magnetic field strength in the region of the electrodes. The increased magnetic field causes the generator voltage to increase, thereby increasing the electrical power produced by the generator. The process of utilizing a portion of the generator output to increase the field strength and thereby increase generator output is

called self-excitation and is used in the operation of all commercial power generators.

The primary technical problem addressed in this program was accomplishing the self-excitation process on a micro-second time scale. The successful operation of a high-power self-excited MHD generator for driving an exploding wire requires a careful design and integration of the explosive and gasdynamic system with the electrodes, self-excitation coils and load characteristics. A combined analytical and experimental effort was conducted to match the electrical parameters of the generator with gasdynamic flow parameters in such manner as to maximize the electrical energy delivered to an exploding wire. Significant effort was expended to determine the electrical and flow properties of the gas and to understand their role in the rapid self-excitation MHD interaction.

3. EXPERIMENTAL STUDY OF EXPLOSIVE MHD GENERATOR

3.1 Gasdynamic Design and Performance

3.1.1 Explosive Driver

The purpose of the explosive driver is to transfer explosive energy to a selected driver gas, shock-compressing it to a high-temperature electrically conducting plasma state. Efficiency of the energy transfer process is an important factor for large tests, as it affects the amount of explosive required per unit of simulator source yield, but is less important for smaller tests. Our approach in this program was to select a relatively simple non-optimum driver configuration with limited efficiency and concentrate effort on the MHD process.

Prior experience has indicated that a driver comprising an aluminum expansion tube and a steel outer tube is moderately effective. Aluminum can expand substantially without rupture, and aluminum-steel impact pressures are sufficiently high to overcome boundary layer stagnation pressures in the driver gas, which may be many times higher than design shock pressure. For a given design, maximum efficiency is obtained by operating the driver at as high a pressure as possible; the limit is governed by loss of gas seal at high shock pressures.

Driver configuration for the program is shown in Figure 3.1, and design parameters based on the assumption of minimal

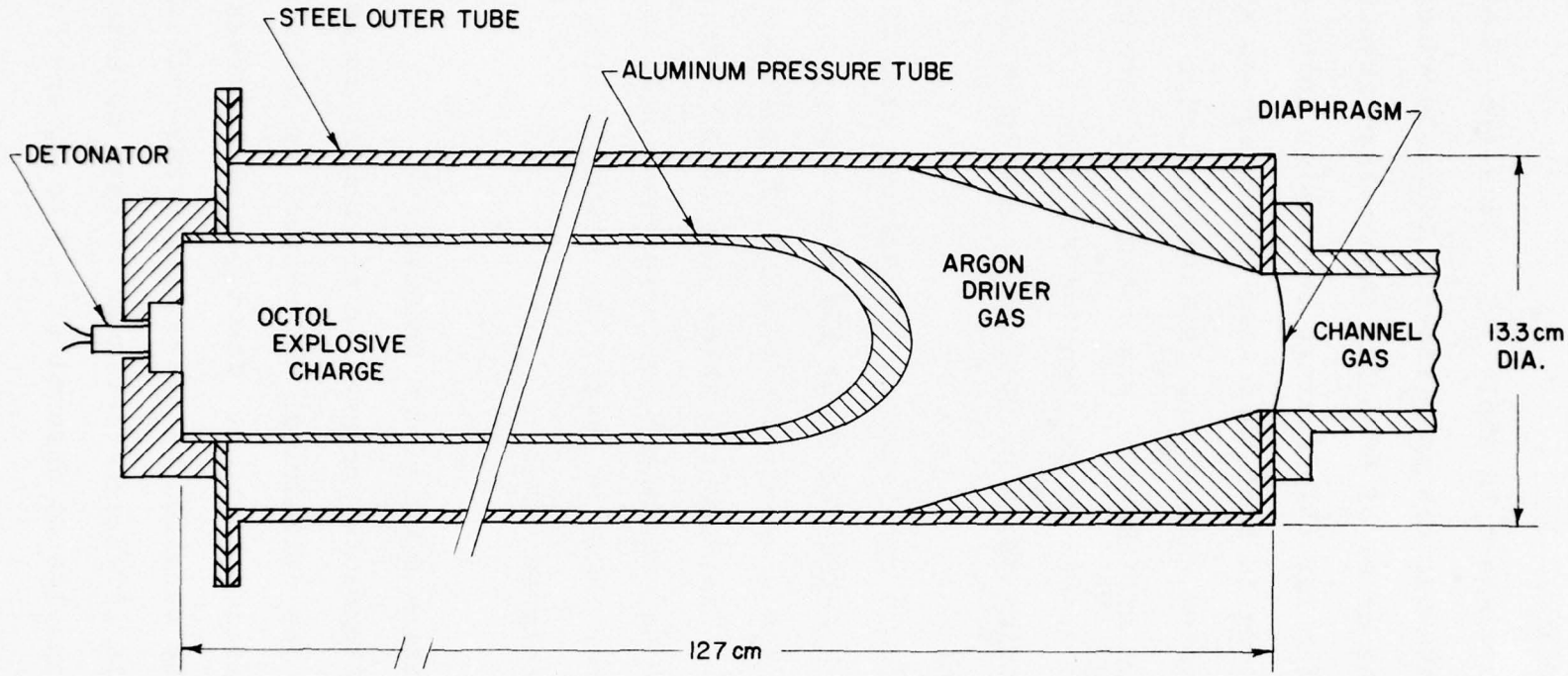

FIGURE 3.1 SCHEMATIC OF EXPLOSIVE DRIVER

gas leakage are shown in Table 3.1. Data from Shot 120-1, which had a 10-kbar design pressure, indicate excessive gas leakage on the order of 40-50%. Rather than investigate the specific reason for this leakage the design shock pressure was reduced from 10 kbar to 6 kbar in subsequent shots. This modification reduced the leakage, although it also reduced design efficiency. Gas leakage was determined by comparing the actual shock location with ideal shock location based on Hugoniot shock relationships and known geometric configurations.

With minimal gas leakage, the drivers used in Shots 120-2 to 120-4 delivered about 10% efficiency, or 10 pounds of explosive yield required per pound of equivalent plasma energy yield. The Hugoniot shock jump conditions determine the plasma state, and since measured shock velocity in the driver was very close to ideal, the plasma conditions were close to calculated values.

3.1.2 Transition Section and Channel

Driver plasma is produced in an annular shape, and is delivered to the cylindrical MHD channel by means of a tapered transition section. The taper also serves to increase pulse duration by decreasing cross-sectional area. Shots 120-1 to 120-3 were designed to have an area reduction from driver annulus to channel of 3.3 to 1, and Shot 120-4,

TABLE 3.1 EXPLOSIVE DRIVER DESIGN PARAMETERS

Shot Number	Working Gas	Loading Density (g/cm^3)	Shock Pressure (kilobars)	Efficiency (percent)	Energy Content of Shocked Gas (Megajoules)
120-1	Argon	1.21×10^{-2}	10.0	18	6.5
120-2	Argon	7.38×10^{-3}	6.0	11	4.0
120-3	Xenon	7.38×10^{-3}	6.0	11	4.0
120-4*	Xenon	7.38×10^{-3}	6.0	10	12.7

*Scaled up approximately 50% in linear dimensions.

in an attempt to increase pulse duration even more to compensate for low plasma conductivity, had an area reduction of 7.2 to 1.

The driver plasma pulse was further processed by expansion into the channel prior to interaction with the MHD generator. Expansion serves the dual purpose of increasing pulse duration and increasing velocity of the leading edge of the pulse, both of which are important for self-excited operation. Shots 120-1 to 120-3 were fired with 1-atm flushed argon initially in the channel, and 120-4 was fired with 0.25-atm air to increase peak velocity still further.

Initial performance predictions of the transition section and channel were preformed by using isentropic nozzle relationships for the channel. More detailed analysis was made using a one-dimensional finite-difference code with variable area option. Typical computed flow speed histories at several channel locations are presented in Figure 3.2.

3.1.3 Performance Data

Performance of driver and transition section gasdynamics were established experimentally by analyzing time-of-arrival data on position-time plots of the shot, as typified by Figures 3.3 and 3.4. Time of arrival was established by self-shorting cap pins in the driver and by various channel diagnostics. As noted above, the driver shock velocity

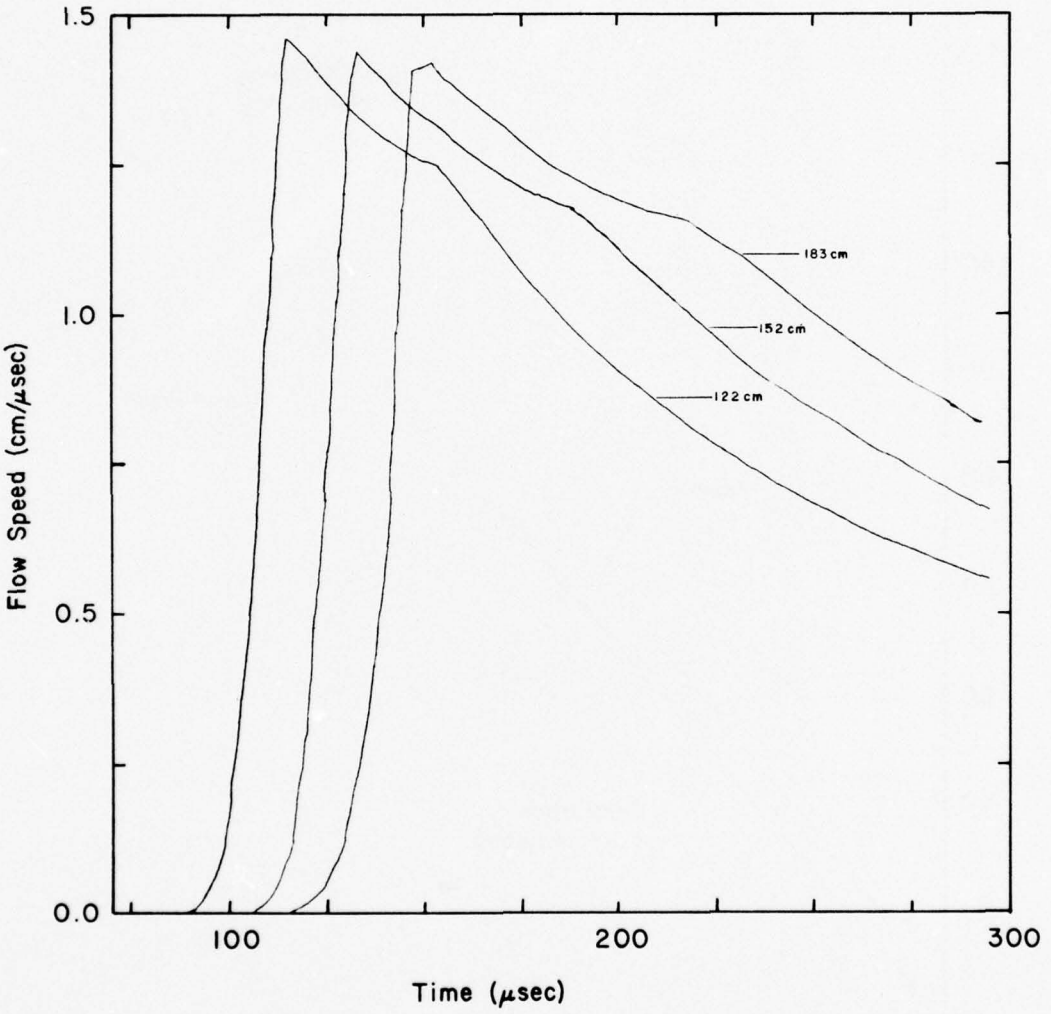

FIGURE 3.2 CALCULATED FLOW SPEED VERSUS TIME IN THE MHD CHANNEL AT SEVERAL AXIAL DISTANCES FROM THE DIAPHRAGM FOR SHOT 120-4

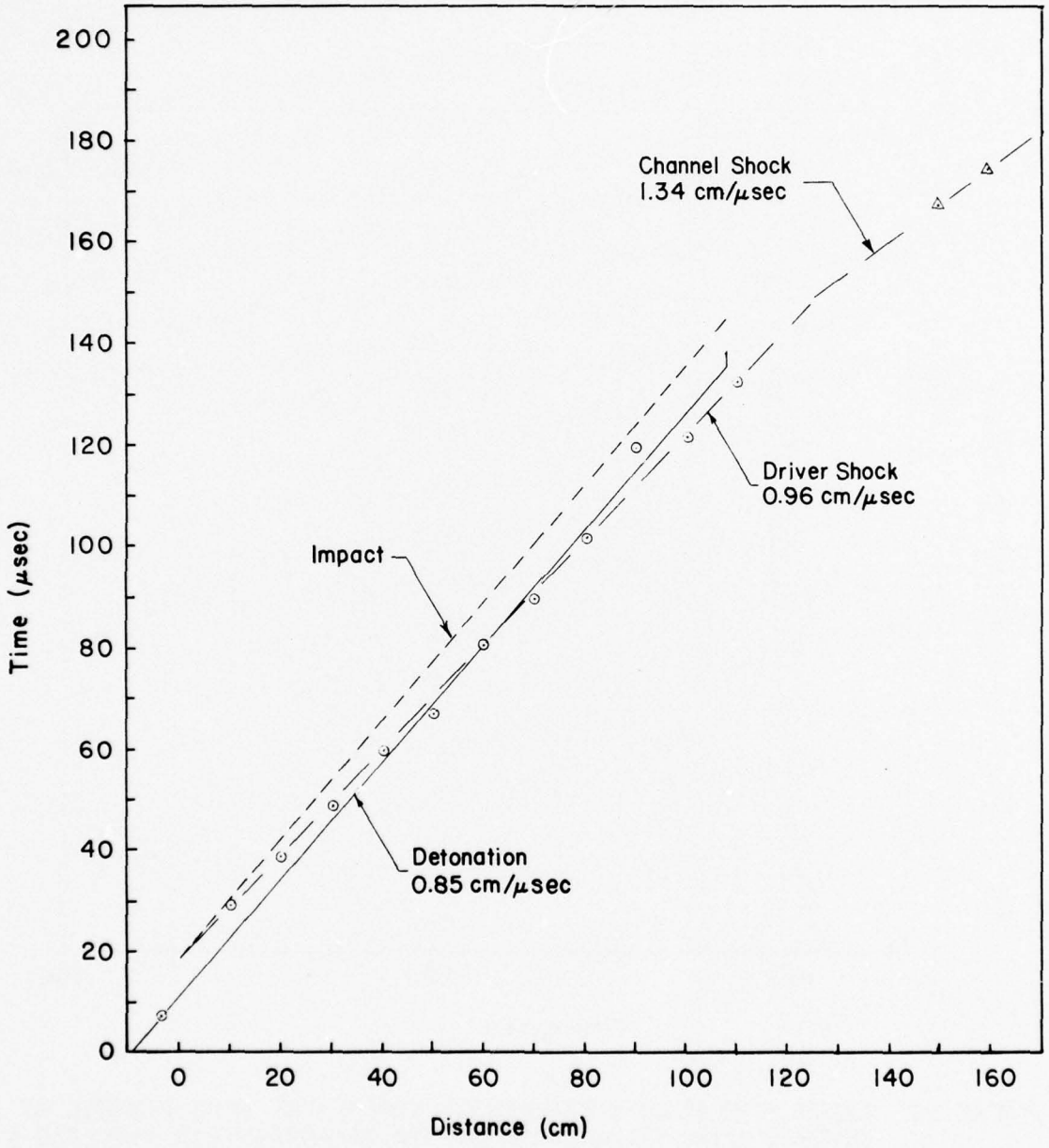

FIGURE 3.3 POSITION-TIME DIAGRAM FOR SHOT 120-2

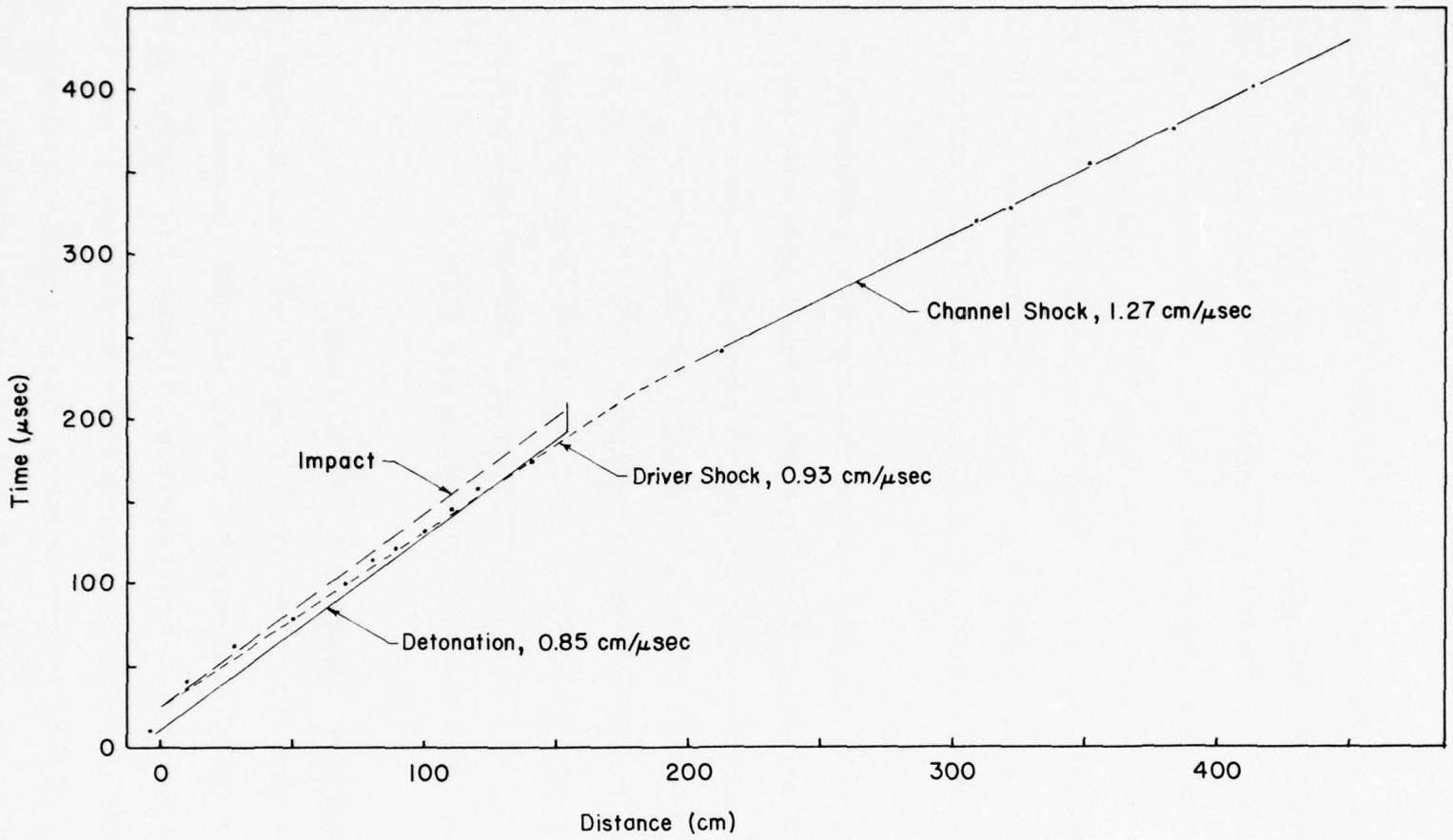

FIGURE 3.4 POSITION-TIME DIAGRAM FOR SHOT 120-4

was close to the calculated values. Shock propagation through the transition section into the channel was found to be slower than the finite difference code calculations, probably because the one-dimensional modeling inadequately represented the two-dimensional interactions in the transition section. Although this source of inaccuracy should eventually be eliminated, it caused only minor inconvenience in the present program, as measured velocities were used to estimate MHD performance.

Velocity history in the channel was obtained with a magnetic velocity gage (an open-circuit MHD generator). A typical velocity gage record is shown in Figure 3.5. The plasma pulse is smooth, with reasonable duration, and appears suitable for MHD power generation. Shot 120-4 was an increase of about 50% in size scale to lengthen pulse duration. The data verify that the driver gasdynamics performed equally well at the larger scale.

3.2 Generator Design and Performance

The principle technical problem foreseen in this program was rapid self-excitation of the MHD generator. In order to convert a reasonable portion of gas energy into electrical energy, it is necessary to provide a very strong magnetic field, on the order of 10-50 tesla. Although it is possible to provide this field with external energization

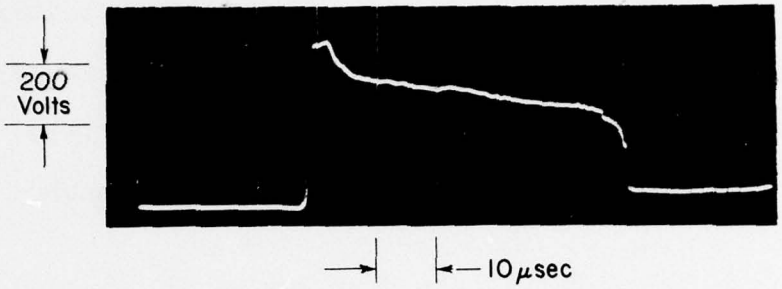

(a) Oscilloscope Record

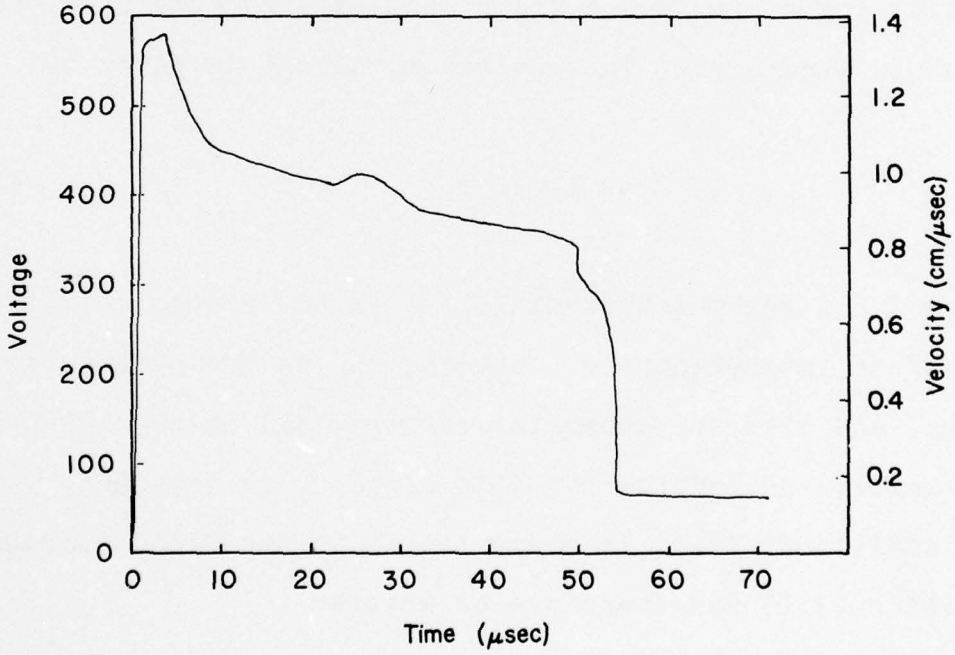

(b) Flow Speed Versus Time

FIGURE 3.5 VELOCITY GAGE RECORD FOR SHOT 120-3

(e.g. a capacitor bank or another explosive MHD generator), the practical requirements of large scale field tests strongly favor self-excitation. With self-excitation an initial field provided by permanent magnets or an external capacitor bank can be amplified to the desired operating field. All commercial rotary generators operate in this manner.

3.2.1 Single-State Analysis

The technical problem areas in devising an effective self-excitation circuit are most reacily introduced by considering a simple one-stage self-excited generator, as shown in Figure 2.2 The generator voltage is given by

$$V = Bub - R_p I \tag{3.1}$$

where B is the magnetic field, u is the plasma velocity, b is the interelectrode distance, R_p is the plasma resistance, and I is the generator current, all in consistent MKS units. An initial magnetic field B_0 is provided, and any additional field is proportional to the field current. Equation (3.1) can therefore be written

$$V = V_o + (Z - R_p)I \tag{3.2}$$

where $V_o = B_o ub$. The parameter Z is the incremental ratio

of open circuit voltage to field coil current, and represents a feedback resistance from output to input.

Applying the generator to an inductive load, we have

$$V = L\frac{dI}{dt} + R_L I \tag{3.3}$$

or

$$L\frac{dI}{dt} = (Z-R)I + V_0 \tag{3.4}$$

where $R = R_p + R_0$ is the total circuit resistance and L is the total circuit inductance.

The generator self-excites if $Z > R$, i.e. the feedback resistance exceeds the circuit resistance. The solution of Equation (3.4) is

$$I = \frac{V_0}{Z-R}\left\{\exp\left[\frac{(Z-R)t}{L}\right] - 1\right\} \tag{3.5}$$

$$\frac{V}{V_0} = \frac{B}{B_0} = \exp\left[\frac{(Z-R)}{L}t\right] \tag{3.6}$$

The self-excitation process will continue until the power drawn is a significant fraction of the thermal power of the plasma, at which point the velocity (and hence Z) will

decrease. This slowdown, usually associated with shock waves in the flow, is known as choking. It has been shown in large non-equilibrium MHD generators that a power extraction rate of approximately 20% can be achieved without serious choking effects (Reference 3.1). This same extraction rate was used as an upper limit in our performance calculations, recognizing that the very different plasma conditions in a high density equilibrium MHD generator may alter this assumed rate limit.

The principal technical problem is to obtain a combination of V_0 , Z , R , and L to achieve choke conditions before the plasma pulse passes through the generator. V_0 depends on the initial field, Z depends on the product of field coil B/I ratio and plasma velocity, R depends principally on plasma conductivity, and L is a field coil parameter. Circuit design concentrates on field coil B/I and L , and gasdynamic design concentrates on plasma pulse duration, velocity, and conductivity.

Considerable engineering effort was expended designing the field coil assembly to minimize L and maximize B/I . Final measured parameters for the 2-inch channel size are L = 70 nanohenry, B/I = 1.2×10^{-5} tesla/amp. At a velocity of 1 cm/microsecond this value of B/I corresponds to Z = 5 milliohm. Coil resistance is a small fraction of a milliohm, and is negligible compared to Z . If plasma resistance were

also negligible, the field doubling time would be

$$\tau = \frac{L}{Z} \ln 2 = 9.7\mu\text{sec} \qquad (3.7)$$

Plasma resistance, if it is too large, has a major effect on field amplification for a given plasma pulse duration. Resistance is related to plasma conductivity by a measured geometrical factor: $R = .28/\sigma$, where σ is measured in mho/cm. The theoretical value of σ is about 400 mho/cm, corresponding to $R = 0.7$ milliohms, low enough not to be a factor. At $\sigma = 50$ mho/cm, $R = 5.6$ milliohms and the plasma resistance would overcome the feedback resistance and self-excitation would not occur. Intermediate values lead to self-excitation of the fields but at a longer time scale. At 100 mho/cm, for example, $R = 2.8$ milliohm and

$$\tau = \frac{L}{Z-R} \ln 2 = 32\mu\text{sec} \qquad (3.8)$$

For a given pulse duration field amplification depends exponentially on the doubling time, which is a function of plasma conductivity. Calculated field amplification for a 100 microsecond pulse duration is shown in Figure 3.6. With conductivities anywhere near theoretical, there is more than enough field amplification to ensure choke conditions even

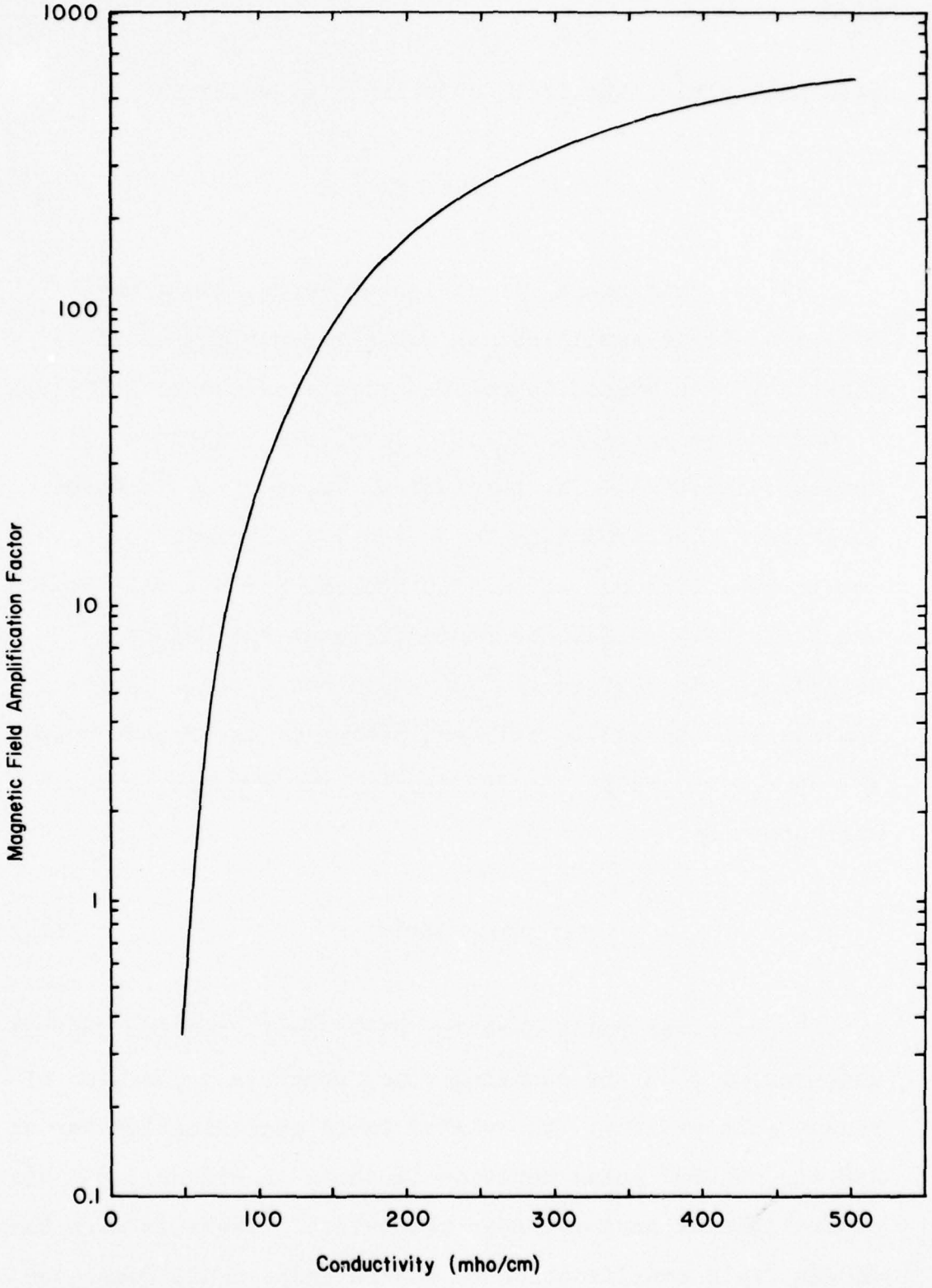

FIGURE 3.6 SINGLE-STAGE FIELD AMPLIFICATION vs. PLASMA CONDUCTIVITY

from a small initial field. Low conductivities on the order of 100 mho/cm lead to greatly reduced amplification, and the actual value is highly sensitive to achieved conductivity.

Although analysis of multi-stage circuits with time-varying parameters is more complex than the single-stage analysis described above, the basic principles and conclusions remain valid. In particular, the generator performance is more or less independent of plasma conductivity above 200 mho/cm but is exponentially affected for conductivities on the order of 100 mho/cm or less.

3.2.2 Generator Design

Channel design is basically a problem of material selection. It was initially required that the channel wall material be an electrical insulator and be sufficiently ductile so as not to rupture on expansion. Lexan filled these requirements, and was used on Shots 120-1, -2, and -3. Later the constraint on ductility was relaxed, as the entire channel was cast in high-density Hydrostone plaster, and wall material was selected on the basis of minimal reduction of plasma conductivity by ablation products. On the basis of chemical equilibrium calculations in the plasma, hydrocarbons were shown to be a poor material, and silicon dioxide was found to be better. A glass channel was used in 120-4.

Expansion of the channel by plasma pressures ($\sim$1 kbar) was found to be excessive in Shots 120-1 and 120-2, which were tamped by a layer of PVC. Shot 120-3 used Plaster of Paris for tamping, and 120-4 used Hydrostone, or high quality, high density plaster. The plaster tamping was found to be effective in preventing channel expansion.

The MHD channel portion of Shots 120-1 and -2 was intended solely to measure the flow speed and gas conductivity (See Figure 3.7). An externally excited field coil provided the magnetic field for an open circuit voltage measurement (velocity gage) and a loaded voltage measurement (plasma conductivity). Since generator power handling was not a design consideration, simple button electrodes were used.

Shot 120-3 was designed not only to measure conductivity but also to use the generator to excite a field coil and use this field in turn to drive a load (See Figure 3.8). To maximize the gas conductivity all hydrocarbons were eliminated in the driver section, and xenon gas was used instead of argon. Electrodes were designed to protrude sufficiently into the flow to penetrate the boundary layer, and were streamlined to minimize leading edge ablation. The electrodes were fabricated from copper blocks to minimize circuit resistance. In anticipation of a gas conductivity of approximately 400 mho/cm the load was designed to match the expected inter-

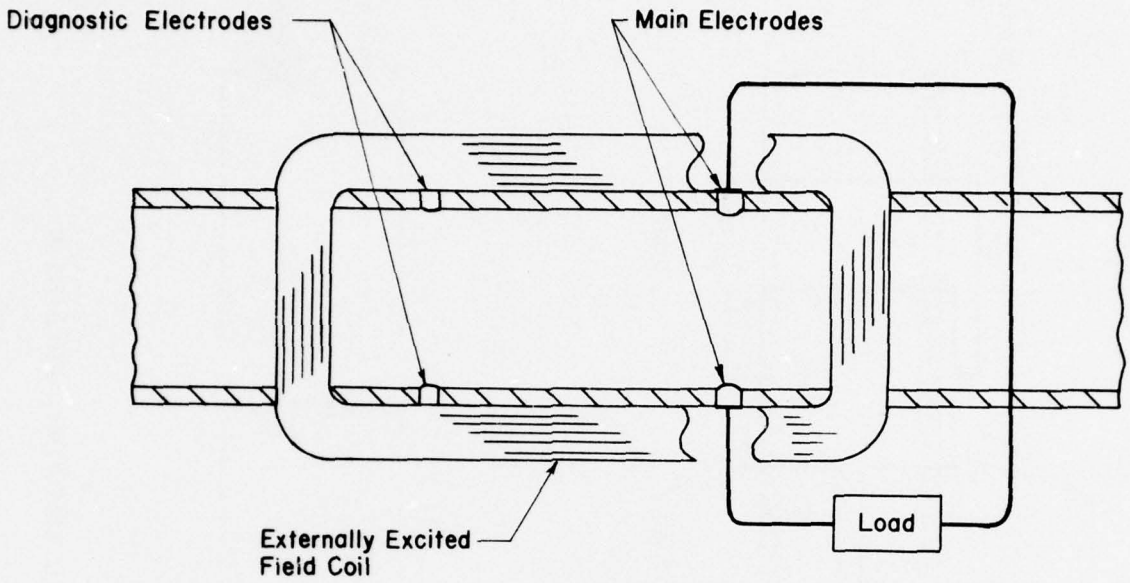

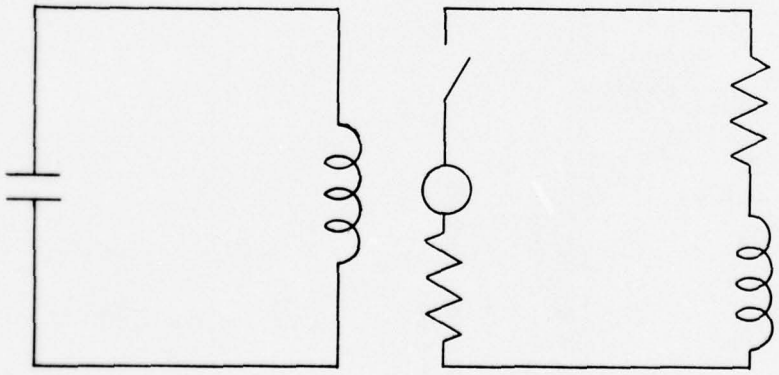

FIGURE 3.7 SCHEMATIC OF MHD CHANNEL CIRCUITRY, SHOTS 120-1 AND 120-2

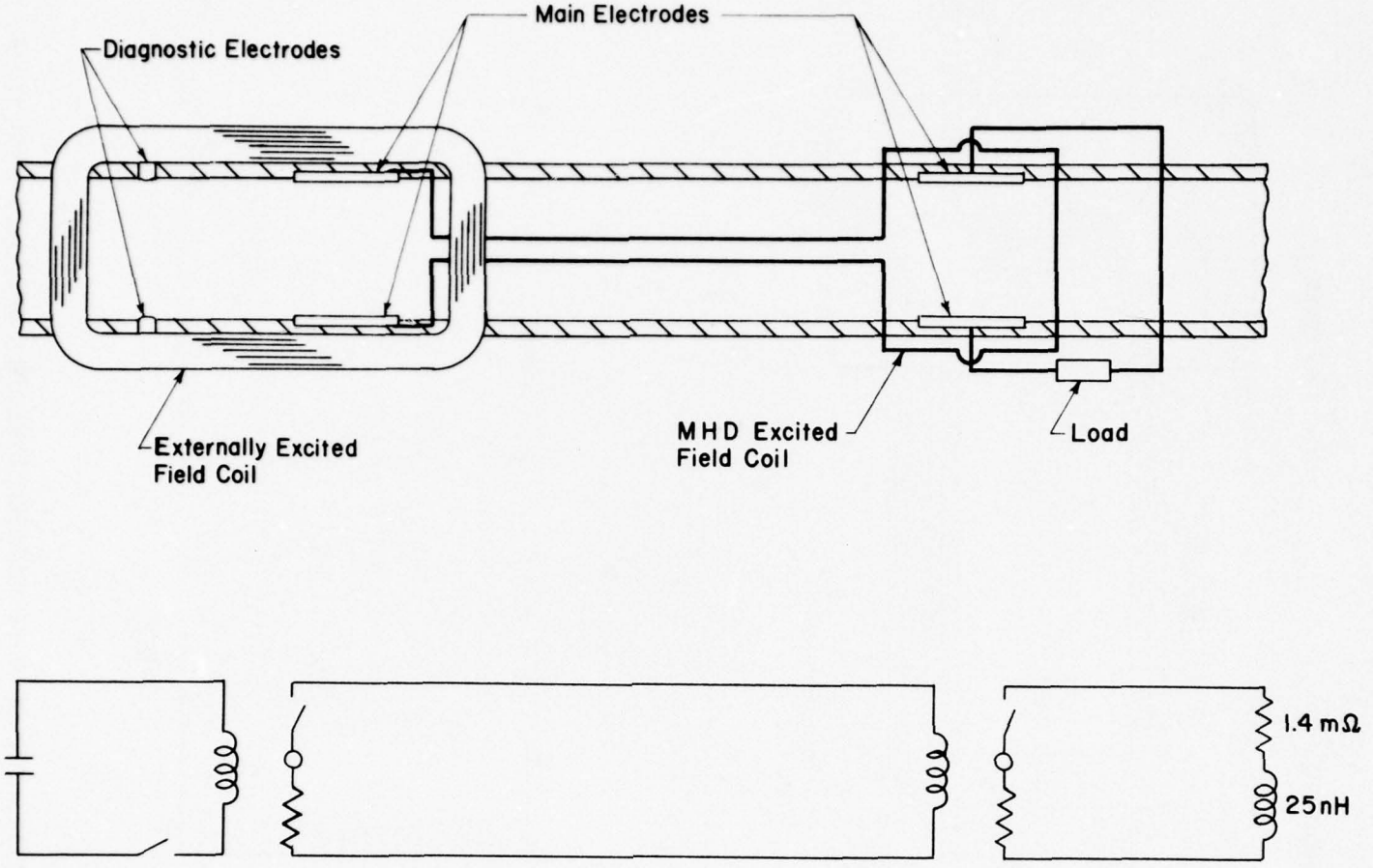

FIGURE 3.8 SCHEMATIC OF MHD CHANNEL CIRCUITRY, SHOT 120-3

electrode plasma resistance of 1.4 milliohms in order to maximize the energy transfer.

Shot 120-4 was designed to obtain full self-excitation and an efficient extraction of energy from the flowing gas. To this end it consisted of five switched, parallel, self-excited stages with a start-up field on the first stage as shown in Figure 3.9. Having multiple stages arranged sequentially along the channel and connected electrically in parallel effectively increases the generator pulse duration as seen by the circuit, and helps to reduce the requirements on plasma conductivity. Circuit switching achieved by split electrodes assures optimum generator loading for self-excitation, and prevents overloading difficulties at early times, when, for example, one generator would otherwise be driving all five field coils. Although the circuit equations are complex, with time varying plasma resistance, feedback resistance, and switching of multiple stages, conventional circuit analysis techniques are applicable.

Electrode design of 120-4 was modified in a further attempt to reduce the observed plasma resistance. The electrodes were finned to penetrate the channel wall boundary layer. They were also plasma-sprayed with tungsten carbide on the basis of calculations showing that ablation vapor of tungsten is substantially more conductive (a factor of three) than the ablation vapor of brass.

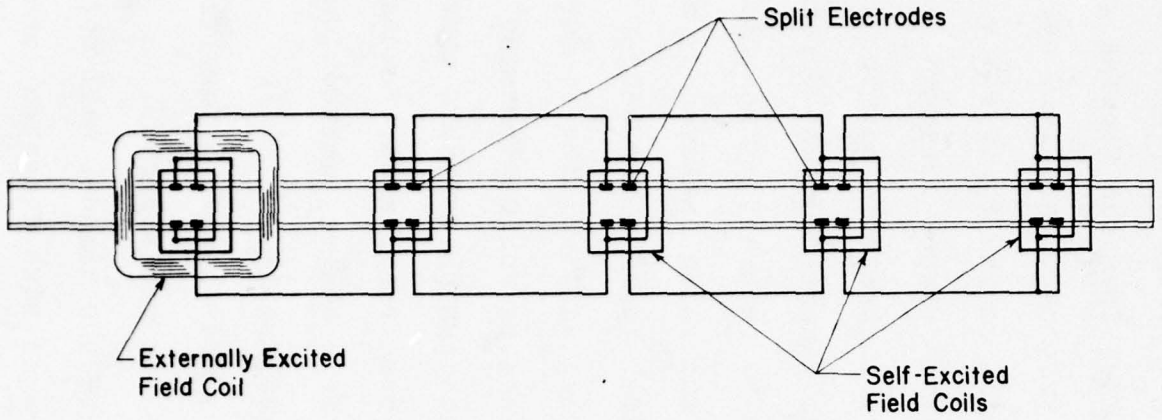

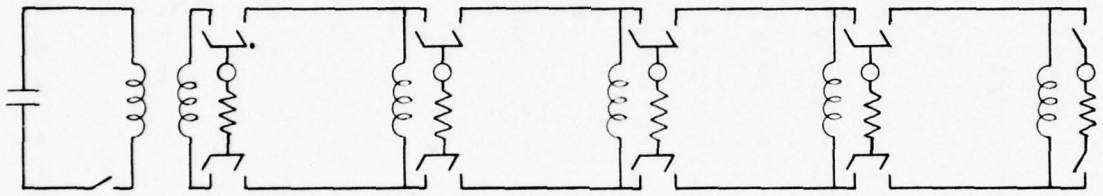

FIGURE 3.9 SCHEMATIC OF MHD CHANNEL CIRCUITRY, SHOT 120-4

To minimize losses in external circuitry (and to prevent excessive heating) resistances were kept as small as possible. At the same time risetime considerations meant inductances were to be kept small and skin effect problems had to be dealt with. These considerations led to the use of wide, flat copper braid and wide, thin copper foil in field coils, loads, and various interconnections. The start-up coil and other field coils were kept as small as possible, consistent with having a sufficiently uniform field in the electrode portion of the channel, to maximize the magnetic field strength per unit current flowing in the coil.

Examples of the experimental hardware for Shot 120-3 are shown in Figure 3.10. Figure 3.10 (a) shows the MHD channel before it was cast in plaster, and Figure 3.10 (b) shows the driver and channel of Shot 120-3 assembled in the field just prior to firing. Figure 3.11 shows generator details of 120-4, including field coil, interstage circuitry, and electrode details. Figure 3.12 shows the MHD channel as assembled prior to casting and as fired.

3.2.3 Performance Data

Performance of the generator depends upon an effective interaction between plasma parameters and circuit elements. The resistance and inductance of each circuit element was measured in the laboratory prior to each shot, while the gas

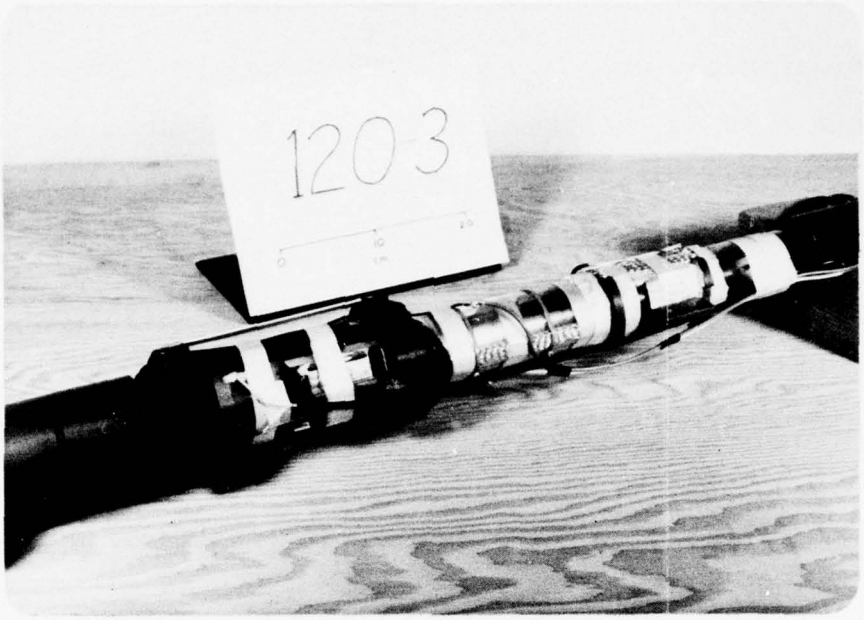

(a) MHD Channel With Coils And Diagnostic Cables In Place Ready For Potting In Plaster

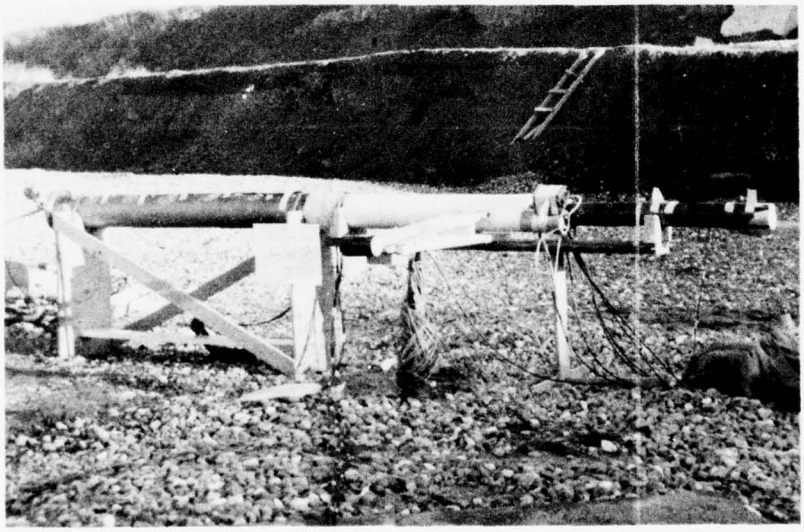

(b) Driver And Channel Assembly On Shot Stand Ready For Firing

FIGURE 3.10 PHOTOGRAPHS OF EXPLOSIVE DRIVER AND MHD CHANNEL, SHOT 120-3

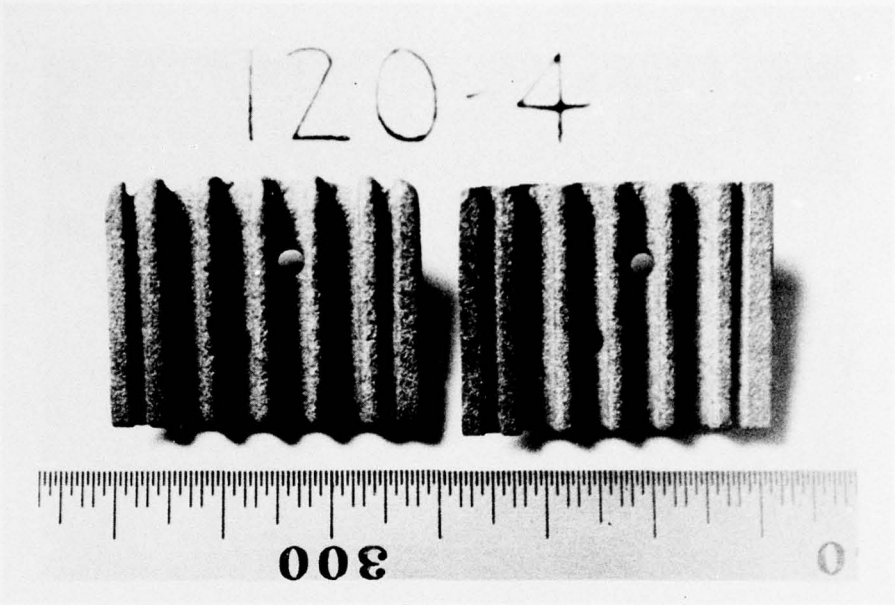

(a) Tungsten-Coated Finned Electrode Detail

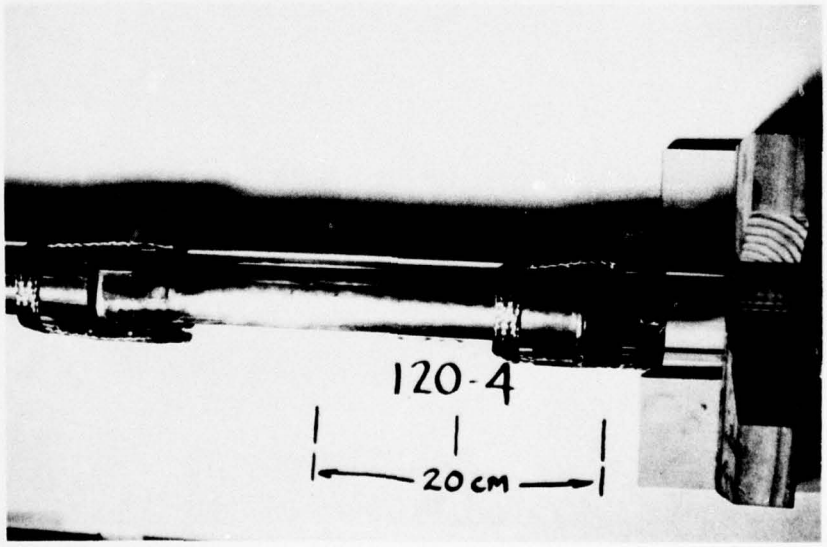

(b) Detail of Stages 3 and 4 Showing Field Coils and Low Inductance Busbar Connections

FIGURE 3.11 GENERATOR DETAIL PHOTOGRAPHS, SHOT 120-4

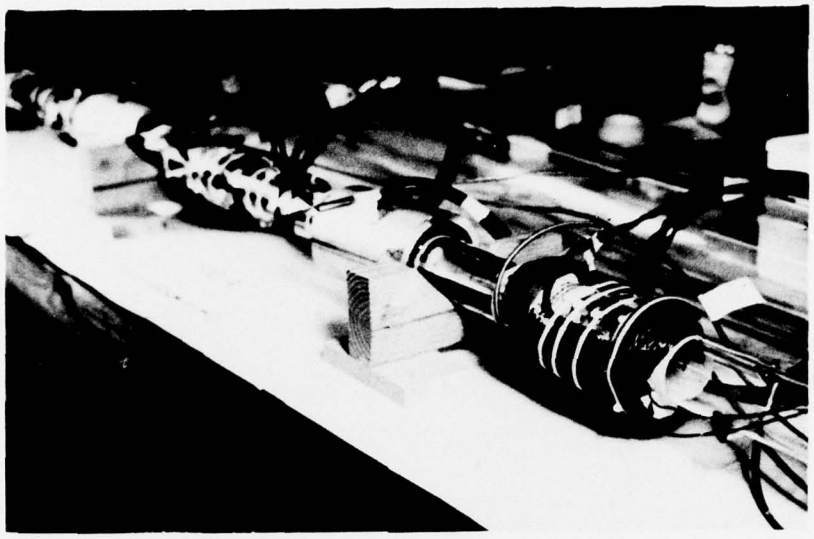

(a) Final Electrical Assembly Prior to Casting

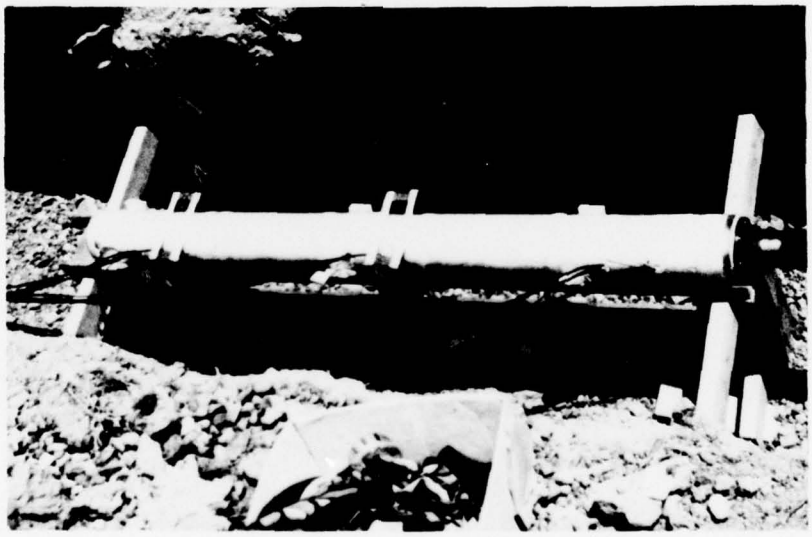

(b) MHD Assembly Prior to Firing

FIGURE 3.12 ASSEMBLY PHOTOGRAPHS, SHOT 120-4

velocity-history in the MHD channel was measured during each shot. Channel measurements also included the time-dependent voltage and current at each electrode station. From this data and a knowledge of the equivalent circuit of the MHD generator circuitry it was always possible to determine a unique plasma resistance as a function of time. This self-consistency provided support for our understanding of the generator behavior and ability to predict electrical response for different generator and circuit parameters. Measured plasma shock velocity and flow duration in the driver were within 10% of predicted values. From these measurements and the equation of state the thermodynamic state of the plasma is accurately known. Plasma velocity increase in the convergent section was found to be overestimated by preshot one-dimensional calculations, particularly when the area convergence was larger than a factor of five. This effect was not unexpected and did not cause problems in circuit design.

Full excitation, up to about 50 tesla choke conditions, was not achieved in this program. The difficulty is clearly attributable to the plasma conductivity, which was found to be substantially less than theoretical calculations. The low conductivity leads to a reduced rate of self-excitation of the magnetic field, and affects exponentially the delivered power or energy for a given plasma pulse duration. Achieved

field amplification of about 10, from .37 to 3.6 tesla, demonstrated the concept of a self-excited generator, but failed by a factor of 15 to achieve choke. On a logarithmic scale, which is appropriate for the exponential amplification process, the achieved gain of 20 dB was about half the required gain of 43 dB. Although the power output was impressive -- about 200 megawatts -- and broke all world records for MHD power production, it was substantially less than peak design levels of about 50 gigawatts. Power increases with the square of the achieved magnetic field, and full power levels can only be reached at full field excitation.

Initial theoretical conductivity calculations were based on the theory of Spitzer and Harm for a fully ionized low density plasma (Reference 3.2), as modified later by Rogov (Reference 3.3) and DeVoto (Reference 3.4). Careful experimental measurements of the conductivity of shocked argon in a shock tube (Reference 3.5) showed excellent agreement with theory up to the maximum achievable shock conditions in that facility (a temperature of 14,000° K and a conductivity of about 80 mho/cm). This accumulated experimental evidence and the agreement among theoretical calculations indicated that theoretical conductivity should be accurate to well within 30%.

A literature survey conducted under different sponsorship after technical completion of this effort revealed a

significant Soviet research effort on dense plasmas at conditions very similar to our experiments. The focal point of the Soviet effort is a major review article by G. E. Norman (Reference 3.6). Subsequent papers by other authors have communicated both experimental and theoretical investigations of dense plasma properties. Cesium was used in many of these investigations because it is relatively easy to achieve the desired plasma conditions. Some work is also reported on argon and xenon plasmas.

Average conductivity was determined from direct electrode-to-electrode resistance measurements, relating this value to conductivity by means of an electrode constant determined from measurements using copper sulfate soultion. Electrode resistance was obtained directly from voltage and current measurements at the electrode. Table 3.2 compares the calculated and measured values of conductivity for the tests in this program.

TABLE 3.2 COMPARISON OF PEAK CONDUCTIVITY VALUES

Shot Number	120-2	120-3	120-4	Units
Theory	307	423	257	mho/cm
Experiment	39	75	82	mho/cm
Ratio	.13	.18	.32	

Observed low conductivity, and the problems deriving from this fact for self-excitation circuit design, led to a progressive series of modifications in shot design. The most likely source of problems is flow contamination from ablating wall materials in the driver, transition section or channel. Extensive calculations of thermochemical equilibrium indicated that wall material made a substantative difference in the conductivity of contaminated plasma. In particular, it was found that the hydrogen in hydrocarbons poisoned the flow by injecting a large number of atoms per unit mass ablated; equipartition demands that energy be shared equally, and hydrogen atoms rob energy otherwise available for ionization. Ablated metal vapor, on the other hand, did very little to reduce conductivity. The reduction in temperature was more than equalized by the increase in ionization of the metal atom. Conductivity of the driver gas could also be increased by using xenon instead of argon.

The progressive changes in driver and channel design to minimize contamination and boundary layer effects are described earlier in this section. It appears that elimination of plastic (hydrocarbon) material in the taper section and changing from argon to xenon caused a factor of two improvement in observed conductivity, whereas further improvements relating to boundary effects at the channel wall and the electrodes resulted in no significant improve-

ment in observed conductivity. The likely cause of the problem therefore, although the data is scanty, is plasma contamination probably occurring in the driver.

There were no apparent problems in the electrical circuit or in the performance of the generator given the measured values of plasma velocity and conductivity. The data can be summarized by saying there were no surprises; generated voltages and currents were consistent with the measured values of inductance and resistance in the circuit components.

Examples of the measured voltages and currents in Shot 120-3 are shown in Figures 3.13 and 3.14. Electrical schematic of this shot is shown in Figure 3.8, and assembly photographs are shown in Figure 3.10. The load current rises smoothly to 77 kamps in a manner fully consistent with the circuit parameters.

Similar curves for Shot 120-4, which was a five-stage self-excitation circuit (See Figure 3.9) were obscured by an operator-induced noise problem which caused baseline shifts in the oscilloscopes (see discussion below). The backup tape recorder channels provided useful absolute data on Stage 3, and the scope records provided data relative to an unknown baseline for the other stages. Reduced data on the Stage 3 field coil current is shown in Figure 3.15. It rises smoothly from zero to a peak of approximately .29 megamps, corresponding to a field strength of 3.6 tesla. Peak power

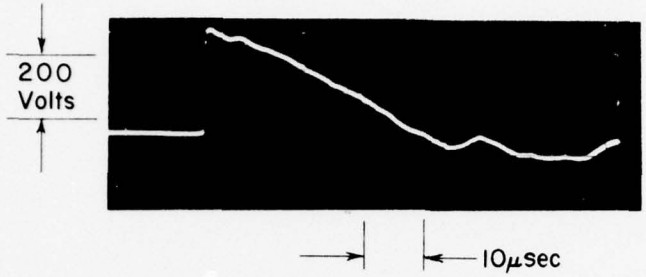

(a) Field Coil Voltage Versus Time

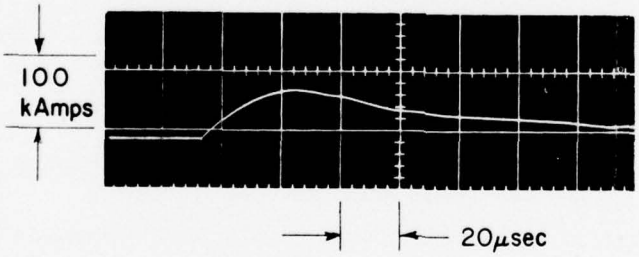

(b) Field Coil Current Versus Time

FIGURE 3.13 MHD EXCITED FIELD COIL VOLTAGE AND CURRENT HISTORIES, SHOT 120-3

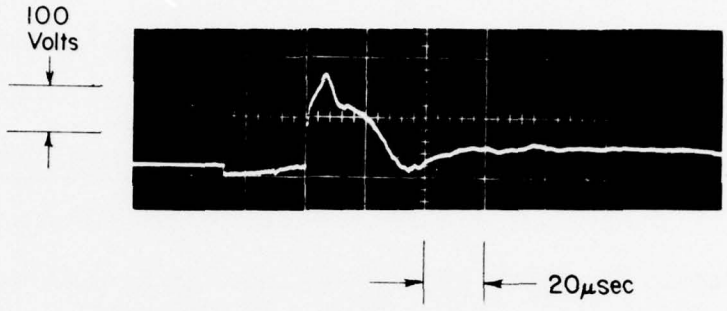

(a) Load Voltage Versus Time

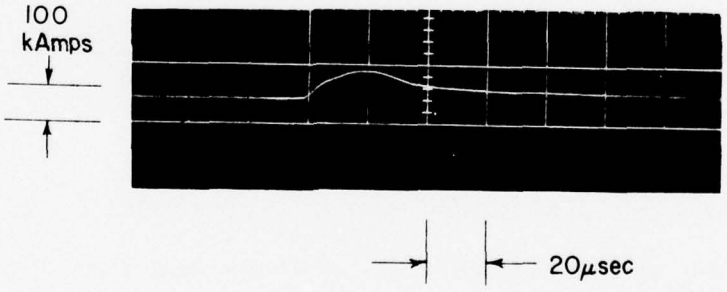

(b) Load Current Versus Time

FIGURE 3.14 LOAD VOLTAGE AND CURRENT HISTORIES, SHOT 120-3

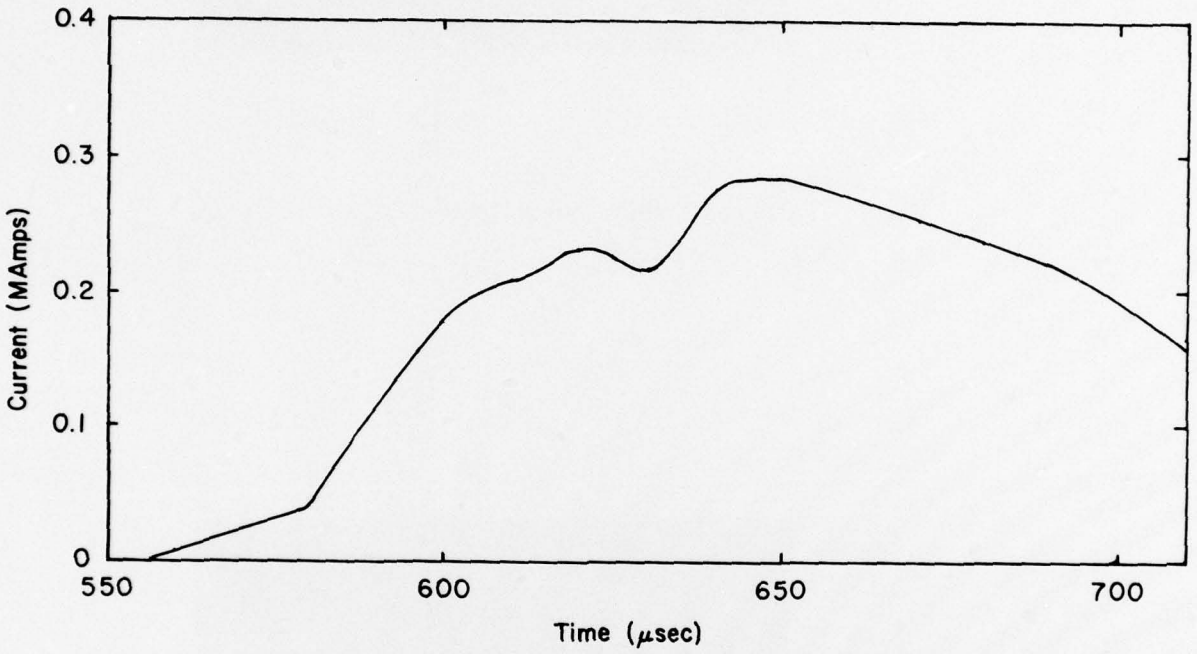

FIGURE 3.15 REDUCED DATA ON STAGE 3 FIELD COIL CURRENT, SHOT 120-4

output of Stage 3 was in excess of 50 megawatts. Total power output from all five stages is conservatively estimated to be in excess of 200 megawatts.

Field amplification did take place in Shot 120-4, but was insufficient to achieve full power output. Initial field on Stage 1 was approximately 0.37 tesla, and peak achieved field in later stages was approximately 3.6 tesla. This amplification factor was consistent with the observed conductivity, but was much less than the factor of 135 required for choke. The peak measured conductivity was only 82 mho/cm, compared with the theoretical value of 257. As shown in Figure 2.6, the amplification factor is very sensitive to marginal conductivity values. Conductivity in excess of 150 mho/cm would very likely have achieved full choke field strengths of about 50 tesla and power levels of about 50 gigawatts.

3.3 Design and Performance of the Diagnostic Devices

Each shot employed at least one small set of electrodes in a magnetic field to measure the velocity of the gas as a function of time. The Faraday open circuit voltage (V) developed across a conductor moving with velocity (u) through a magnetic field (B) is $V = Bub$, where b is the distance between the electrodes. Since B and b are typically known parameters, the open-circuit voltage provides

a direct time-dependent measurement of the velocity of the gas.

Several factors influence the actual performance of the velocity gage. Electrode motion must be small during the gas pulse, otherwise a proper $b(t)$ would have to be included in the analysis. Fringing fields from nearby magnetic field sources must be included in the total B, and in general these might include time-varying fields.

The leads must be isolated from ground or at least isolated from other electrodes in contact with the gas to avoid problems of cross-coupling. This was accomplished by using a wideband isolation transformer between the velocity gage and the grounded oscilloscope. An example of a velocity gage record is shown in Figure 3.5.

Examples of main electrode voltage records are shown in Figures 3.13(a) and 3.14(a). As with the velocity gage the leads of these had to be isolated from ground via wideband isolation transformers, since the main electrodes are likewise in contact with the gas. The only other concern in making these measurements was to arrange the leads so as to minimize inductive pickup, since they were generally in locations of large amplitude, time-varying magnetic fields.

Examples of current measurements are shown in Figure 3.13(b) and Figure 3.14(b). These measurements were made by using solenoidal search coils closely coupled to current

carrying elements. The search coil outputs were then integrated to provide signals proportional to circuit currents as shown. The search coils were calibrated in the laboratory at frequencies corresponding to the MHD circuit current rise-times ($\sim$100 kHz). The essence of the calibration was to measure the mutual inductance between the search coil and the current carrying element. At the frequencies of interest there are negligible capacitive effects, but care had to be taken to minimize stray inductive pickup.

A problem occurred in Shot 120-4 which is worthy of note because it affected the data. Shot 120-4 had numerous diagnostic channels because of the complexity of the electrical circuit; there were five stages, of which three (the first, third, and fifth) weremonitored for field coil current, electrode current, and electrode voltage. In addition there were two velocity gages. All these components were calibrated and checked out in the laboratory. Coupling problems occurred at the test site, which were finally traced down to some combination of ground shift in the capacitor power supply for the first stage saddle coil, and high impedance stray coupling through the Hydrostone casting plaster. It was found that the problem could be eliminated by floating the power supply ground. The technician who fired the shot inadvertently reconnected the ground by simultaneously touching the safety interlock key and the power supply case.

Resulting base shifts affected the oscilloscopes and most of the tapedeck data. The problem could be eliminated in future shots by a firing procedure change, a modification of the power supply, or a careful redesign of the circuit insulation in the Hydrostone casting.

4. CONCLUSIONS AND RECOMMENDATIONS

4.1 Accomplishments

- Designed and successfully tested explosive driver system. Conversion efficiency from chemical energy of explosive to delivered plasma energy was 10%. Largest shot fired was 120-4, which delivered 12 megajoules plasma energy in approximately 100 microseconds, for a total thermal power of 120 gigawatts.

- Designed and successfully tested fast self-excited MHD field coil and circuit assembly, including multiple stage and switched electrodes. Field coil inductance for 2-inch channel was measured as 70 nanohenries.

- Successfully produced MHD power at levels consistent with magnetic field. Peak power was in excess of 200 megawatts with a 3.6 tesla field in Shot 120-4.

- Successfully demonstrated self-excitation consistent with the observed low values of electrical conductivity. Observed field amplification on Shot 120-4 was a factor of

approximately 10, from .37 to 3.6 tesla.

- Successfully developed and tested MHD measurement techniques for monitoring high performance energy flow under explosive field test conditions. Plasma velocity gage and electrode current monitors worked exceptionally well in all shots but 120-4, which had an inadvertent ground loop problem arising from operation procedures at the test site.

4.2 Problems

- Observed average conductivity of the plasma as determined from electrode measurements was substantially smaller than theory (approximately a factor of three). This low value, occurring in an exponential term, prevented achieving full field amplification and full power generation capability. Approximately 43 dB of gain (50 tesla) was required for full power, and 20 dB (3.6 tesla) was actually achieved. An increase of 50% in experimental conductivity would have assured full gain conditions.

- Experimental design modifications improved the measured conductivity, but did not cure the problem. Major improvements followed changing driver gas from argon to xenon, and substituting an aluminum convergent nozzle for a PVC plastic nozzle. Modifications directed toward minimizing boundary layer effects -- changing channel wall material and electrode material and geometry -- did not appear to improve conductivity significantly. A possible source of the problem is contamination of the plasma in the explosive driver by ablated or jetted wall material.

- In general, engineering design and fabrication of circuit components proved to be considerably more complex than initially contemplated. Calibration of the field coil assemblies and MHD instrumentation was also more complex and time-consuming than expected.

4.3 Conclusions

- The principle of self-excited high-energy, high-power MHD electric power generation in explosive tests scalable to large sizes has been demonstrated in this program, but expected and required

levels of self-excitation field gain for full output were not achieved.

- In order to achieve full power output from a self-excited MHD generator the conductivity problem must be solved.

- Externally-excited explosive MHD is a reasonable, practical means for achieving extremely high plasma energy densities for DNA simulation requirements in present and future programs.

4.4 Recommendations

- The conductivity problem can be resolved in either of two different ways: identify and rectify the plasma contamination causing lower than expected conductivity, or go to a convergent driver capable of delivering plasma at higher velocities. Increased MHD feedback impedance at high velocities reduces the requirements on conductivity. For DNA applications it is recommended that the latter convergent driver approach be pursued. This choice has the advantage of operating at increased voltage levels and correspondingly

more rapid self-excitation. It is recommended that a plasma source be developed with plasma properties specifically selected for a self-exited MHD device.

- Having demonstrated a satisfactory plasma source in terms of flow velocity, plasma conductivity and duration, a further effort is recommended for tailoring both the gasdynamics and electrical generator output to satisfy particular DNA simulation requirements. This effort consists of adapting the basic MHD technology to meet the needs of a particular application.

REFERENCES

3.1 B. Zauderer, "Investigation of a Non-Equilibrium MHD Generator", General Electric Company, Annual Report Project Code 9800, 1974.

3.2 L. Spitzer and R. Harm, "Transport Phenomena in a Completely Ionized Gas", Physical Review, Vol. 89, No. 5, pp. 997-981, March, 1953.

3.3 V. S. Rogov, "Calculation of Plasma Conductivity", Teplofizika Vysokikh Temperatur, Vol. 8, No. 4, pp. 689-694, August, 1970; Translation available, Consultants Bureau, Plenum Publishing Co., UDC 533.932.

3.4 R. S. DeVoto, "Transport Coefficients of Ionized Argon", Physics of Fluids, Vol. 16, No. 5, pp. 616-623, May, 1973.

3.5 S. C. Lin, E. L. Resler, and P. Kantrowitz, "Electrical Conductivity of Highly Ionized Argon Produced by Shock Waves", Journal of Applied Physics, Vol. 26, No. 1, pp. 95-109, January, 1955.

3.6 G. E. Norman and A. N. Starostin, "Thermodynamics of a Strongly Nonideal Plasma", Teplofizika Vysokikh Temperatur, Vol. 8, No. 2, pp. 413-438, March-April, 1970; Translation Consultants Bureau, UDC 533.95, 1970.

DISTRIBUTION LIST

DEPARTMENT OF DEFENSE

Assistant to the Secretary of Defense
ATTN: Honorable Donald R. Cotter

Director
Defense Advanced Rsch. Proj. Agency
ATTN: NMRO
ATTN: PMO
ATTN: STO
ATTN: Tech. Library

Director
Defense Civil Preparedness Agency
Assistant Director for Research
ATTN: Admin. Officer

Defense Documentation Center
12 cy ATTN: TC

Director
Defense Intelligence Agency
ATTN: DT-1C
ATTN: DB-4C, Edward O'Farrell
ATTN: DT-2, Wpns. & Sys. Division

Director
Defense Nuclear Agency
ATTN: TISI, Archives
ATTN: DDST
3 cy ATTN: TITL, Tech. Archives
2 cy ATTN: SPSS

Chairman
Dept. of Defense Explo. Safety Board
ATTN: DD/S&SS
ATTN: Thomas Zaker

Dir. of Defense Rsch. & Engineering
ATTN: S&SS (OS)

Commander
Field Command, Defense Nuclear Agency
ATTN: FCTMOF
ATTN: FCT
ATTN: FCPR

Chief
Livermore Division, Fld. Command, DNA
ATTN: FCPRL

Chief
Test Construction Division
Field Command Test Directorate
Defense Nuclear Agency
ATTN: FCTC

DEPARTMENT OF THE ARMY

Dep. Chief of Staff for Rsch. Dev. & Acq.
ATTN: Tech. Library

Deputy Chief of Staff for Ops. & Plans
ATTN: Technical Library

DEPARTMENT OF THE ARMY (Continued)

Chief of Engineers
ATTN: DAEN-RDM
ATTN: DAEN-MCE-D

Commander
Harry Diamond Laboratories
ATTN: DRXDO-TI, Tech. Library
ATTN: DRXDO-NP

Commander
Redstone Scientific Information Ctr.
U.S. Army Missile Command
ATTN: Chief, Documents

Director
U.S. Army Ballistic Research Labs.
ATTN: J. H. Keefer, DRDAR-BLE
ATTN: Julius J. Meszaros, DRXBR-X
ATTN: Edward Baicy, Tech. Library
ATTN: W. Taylor, DRDAR-BLE

Director
U.S. Army Engr. Waterways Exper. Sta.
ATTN: John N. Strange
ATTN: Guy Jackson
ATTN: Tech. Library
ATTN: William Flathau

Commander
U.S. Army Mat. & Mechanics Rsch. Ctr.
ATTN: Technical Library

Commander
U.S. Army Materiel Dev. & Readiness Cmd.
ATTN: Technical Library

Commander
U.S. Army Mobility Equip. R & D Ctr.
ATTN: Technical Library

Commander
U.S. Army Nuclear Agency
ATTN: Technical Library

DEPARTMENT OF THE NAVY

Chief of Naval Material
ATTN: MAT 0323

Chief of Naval Operations
ATTN: OP 981
ATTN: OP 03EG

Chief of Naval Research
ATTN: Code 464, Jacob L. Warner
ATTN: Code 464, Thomas P. Quinn
ATTN: Nicholas Perrone
ATTN: Technical Library

Officer-in-Charge
Civil Engineering Laboratory
Naval Construction Battalion Center
ATTN: R. J. Odello
ATTN: Technical Library

DEPARTMENT OF THE NAVY (Continued)

Commander
David W. Taylor Naval Ship R & D Ctr.
ATTN: Code L42-3, Library

Commander
Naval Electronic Systems Command
Naval Electronic Systems Cmd. Hqs.
ATTN: PME 117-21A

Commander
Naval Facilities Engineering Command
ATTN: Code 04B
ATTN: Technical Library
ATTN: Code 03A

Director
Naval Research Laboratory
ATTN: Code 2600, Tech. Library

Commander
Naval Sea Systems Command
ATTN: Code 03511
ATTN: ORD-91313, Library

Commander
Naval Ship Engineering Center
ATTN: Technical Library
ATTN: NSEC 6105G

Commander
Naval Ship Rsch. and Development Ctr.
Underwater Explosive Research Division
ATTN: John Gordon
ATTN: Technical Library

Officer-in-Charge
Naval Surface Weapons Center
ATTN: Code WA501, Navy Nuc. Prgms. Off.

Commander
Naval Surface Weapons Center
ATTN: Technical Library

Director
Strategic Systems Project Office
ATTN: NSP-272
ATTN: NSP-43, Tech. Library

DEPARTMENT OF THE AIR FORCE

AF Geophysics Laboratory, AFSC
ATTN: LWW, Ker C. Thompson

AF Institute of Technology, AU
ATTN: Library AFIT Bldg 640, Area B

AF Weapons Laboratory, AFSC
ATTN: DES-S, M. A. Plamondon
ATTN: DES-C, Robert Henny
ATTN: DEX
ATTN: SUL

Headquarters
Air Force Systems Command
ATTN: DLCAW
ATTN: Technical Library

HQ USAF/IN
ATTN: INATA

DEPARTMENT OF THE AIR FORCE (Continued)

HQ USAF/RD
ATTN: RDQSM

Commander in Chief
Strategic Air Command
ATTN: NRI-STINFO Library

U.S. ENERGY RESEARCH AND DEVELOPMENT ADMINISTRATION

Division of Military Application
ATTN: Doc. Control for Test Office

University of California
Lawrence Livermore Laboratory
ATTN: Larry W. Woodruff, L-96
ATTN: Tech. Info. Dept. L-3

Los Alamos Scientific Laboratory
ATTN: Doc. Control for Reports Lib.

Sandia Laboratories
ATTN: Doc. Control for Tech. Library

Sandia Laboratories
ATTN: Doc. Control for Org. 3422-1,
Sandia Rpt. Coll.

U.S. Energy Rsch. & Dev. Admin.
ATTN: Doc. Control for Tech. Library

U.S. Energy Rsch. & Dev. Admin.
Division of Headquarters Services
Library Branch, G-043
ATTN: Doc. Control for Class. Tech. Lib.

U.S. Energy Rsch. & Dev. Admin.
ATTN: Doc. Control for Tech. Lib.

DEPARTMENT OF DEFENSE CONTRACTORS

Aerospace Corporation
ATTN: Tech. Info. Services

Artec Associates, Inc.
ATTN: Dennis W. Baum
ATTN: W. Lee Shimmin
ATTN: Stephen P. Gill

The Boeing Company
ATTN: Aerospace Library

Civil/Nuclear Systems Corp.
ATTN: Robert Crawford

EG&G, Inc.
ATTN: Technical Library

General Electric Company
TEMPO-Center for Advanced Studies
ATTN: DASIAC

IIT Research Institute
ATTN: Technical Library

Institute for Defense Analyses
ATTN: IDA Librarian, Ruth S. Smith

Kaman Sciences Corporation
ATTN: Library

DEPARTMENT OF DEFENSE CONTRACTORS (Continued)

Lockheed Missiles & Space Co. Inc.
ATTN: Technical Library

Lovelace Foundation for Medical Education & Research
ATTN: Technical Library

Physics International Company
ATTN: Doc. Control for Coye Vincent
ATTN: Doc. Control for E. T. Moore
ATTN: Doc. Control for Charles Godfrey
ATTN: Doc. Control for Tech. Library

R & D Associates
ATTN: Technical Library
ATTN: Robert Port
ATTN: J. G. Lewis

Science Applications, Inc.
ATTN: Technical Library

Science Applications, Inc.
ATTN: R. A. Shunk

Southwest Research Institute
ATTN: Wilfred E. Baker
ATTN: A. B. Wendel

DEPARTMENT OF DEFENSE CONTRACTORS (Continued)

SRI International
ATTN: Burt R. Gasten
ATTN: George R. Abrahamson

Systems, Science and Software, Inc.
ATTN: Donald R. Grine
ATTN: Technical Library

TRW Defense & Space Sys. Group
ATTN: Tech. Info. Center, S-1930
ATTN: D. H. Baer, R1-2136
2 cy ATTN: Peter K. Dai, R1-2170

TRW Defense & Space Sys. Group
ATTN: E. Y. Wong, 527/712

The Eric H. Wang
Civil Engineering Rsch. Fac.
ATTN: Larry Bickle
ATTN: Neal Baum

Weidlinger Assoc. Consulting Engineers
ATTN: Melvin L. Baron

Weidlinger Assoc. Consulting Engineers
ATTN: J. Isenberg